JACS
JOURNAL OF THE AMERICAN CHEMICAL SOCIETY
pubs.acs.org/JACS
Article

Role of Electron-Deficient Olefin Ligands in a Ni-Catalyzed Aziridine Cross-Coupling To Generate Quaternary Carbons

Jesús G. Estrada, Wendy L. Williams, Stephen I. Ting, and Abigail G. Doyle*

Cite This: J. Am. Chem. Soc. 2020, 142, 8928–8937
Read Online

ABSTRACT: We previously reported the development of an electron-deficient olefin (EDO) ligand, Fro-DO, that promotes the generation of quaternary carbon centers via Ni-catalyzed Csp^3–Csp^3 cross-coupling with aziridines. By contrast, electronically and structurally similar EDO ligands such as dimethyl fumarate and electron-deficient styrenes afford primarily β-hydride elimination side reactivity. Only a few catalyst systems have been identified that promote the formation of quaternary carbons via Ni-catalyzed Csp^3–Csp^3 cross-coupling. Although Fro-DO represents a promising ligand in this regard, the basis for its superior performance is not well understood. Here we describe a detailed mechanistic study of the aziridine cross-coupling reaction and the role of EDO ligands in facilitating Csp^3–Csp^3 bond formation. This analysis reveals that cross-coupling proceeds by a $Ni^{0/II}$ cycle with a Ni^{II} azametallacyclobutane catalyst resting state. Turnover-limiting C–C reductive elimination occurs from a spectroscopically observable Ni^{II}-dialkyl intermediate bound to the EDO. Computational analysis shows that Fro-DO accelerates turnover limiting reductive elimination via LUMO lowering. However, it is no more effective than dimethyl fumarate at reducing the barrier to Csp^3–Csp^3 reductive elimination. Instead, Fro-DO's unique reactivity arises from its ability to associate favorably to Ni^{II} intermediates. Natural bond order second-order perturbation theory analysis of the catalytically relevant Ni^{II} intermediate indicates that Fro-DO binds to Ni^{II} through an additional stabilizing donor–acceptor interaction between its sulfonyl group and Ni^{II}. Design of new ligands to evaluate this proposal supports this model and has led to the development of a new and tunable ligand framework.

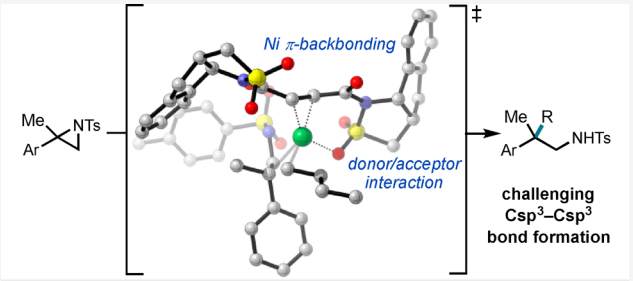

INTRODUCTION

Transition-metal-catalyzed cross-coupling has emerged as the prevailing method for C–C bond formation in a wide range of subdisciplines of chemistry, from medicinal and process chemistry to materials science.[1] While most applications involve Csp^2–Csp^2 cross-coupling, remarkable advances have been described for Csp^2–Csp^3 and Csp^3–Csp^3 bond formation.[2] Nevertheless, Csp^3–Csp^3 cross-coupling remains a considerable challenge, particularly when generating quaternary carbon centers. The comparative lack of success in these cross-coupling reactions can be attributed to a few factors. Reductive elimination is slow because it proceeds from a directional sp^3-orbital and incurs high reorganizational energy during the bond-forming step.[3] Additionally, the alkyl metal intermediate may undergo reversible β-hydride elimination followed by facile C–H reductive elimination, resulting in the overall reduction or isomerization of substrates (Figure 1A).

The use of electron-deficient olefins (EDOs) as ligands in Csp^3 cross-coupling reactions has emerged as a successful approach to address challenges associated with slow reductive elimination and facile β-hydride elimination.[4] These π-deficient ligands have been proposed to serve multiple roles. EDOs can improve product selectivity by deterring β-hydride elimination through occupation of a coordination site (Figure 1B).[5] EDOs have also been shown to accelerate reductive elimination, arising from the ligand's ability to stabilize the buildup of electron density on the metal center in the transition state.[6] Olefin binding may also accelerate reductive elimination through generation of an odd-coordinate complex that undergoes reductive elimination faster than a corresponding even-coordinate complex.[7] In the context of Csp^3–Csp^3 bond formation with Ni, Yamamoto was first to study the impact of olefinic ligands on reductive elimination, using (bipy)$NiEt_2$ complexes as model substrates (Figure 1C).[6] Subsequently, Knochel deployed these ligands in catalysis, demonstrating a Ni-catalyzed Negishi Csp^3–Csp^3 cross-coupling of primary alkyl electrophiles.[8,9] In this case, inclusion of an electron-deficient styrene led to improved product selectivity over side products that are formed in the ligand's absence.[10] These studies set the stage for the application of

Received: February 28, 2020
Published: April 29, 2020

https://dx.doi.org/10.1021/jacs.0c02237
J. Am. Chem. Soc. 2020, 142, 8928–8937

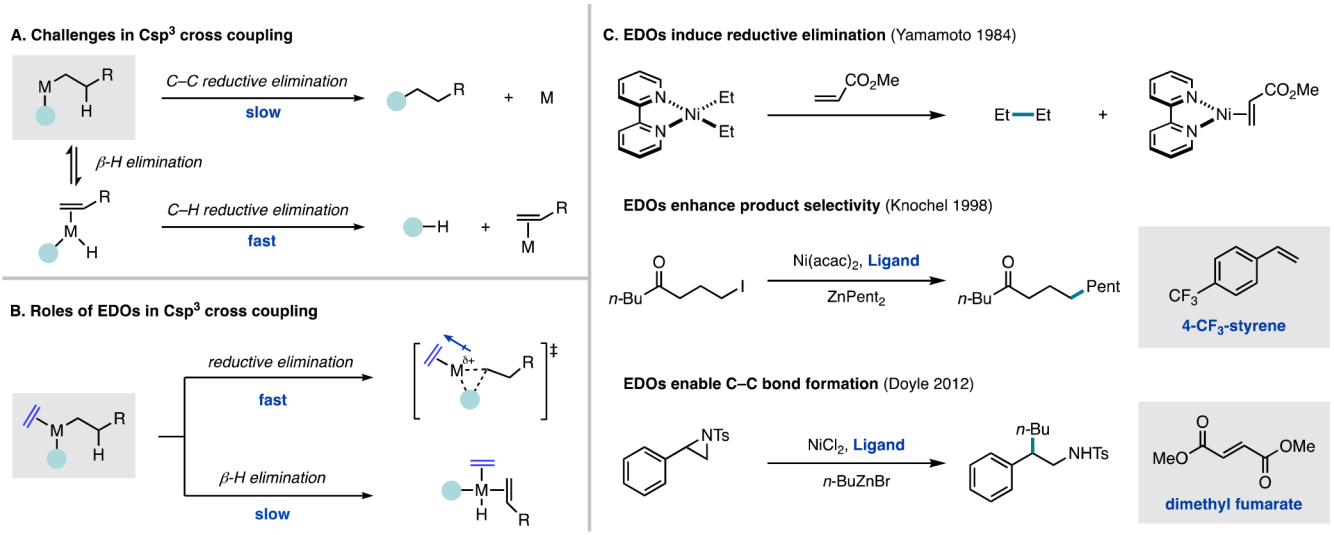

Figure 1. Electron-deficient olefin (EDO) ligands in Ni-catalyzed Csp^3 cross-coupling reactions.

simple fumarate and styrene derivatives as ligands in a range of Ni-catalyzed Csp^3 cross-coupling reactions, including a 2012 study from our group investigating a Ni-catalyzed Negishi Csp^3–Csp^3 cross-coupling of styrenyl aziridines in which dimethyl fumarate was necessary to accomplish Csp^3–Csp^3 bond formation.[11,12]

In 2015, our group reported a Ni-catalyzed Negishi cross-coupling reaction with 2,2-disubstituted aziridines as electrophiles using a novel EDO ligand, Fro-DO (Scheme 1).[13] This

Scheme 1. Ni-Catalyzed Negishi Csp^3–Csp^3 Cross-coupling of 2,2-Disubstituted Aziridine 1 Exhibits Different Selectivity among EDOs

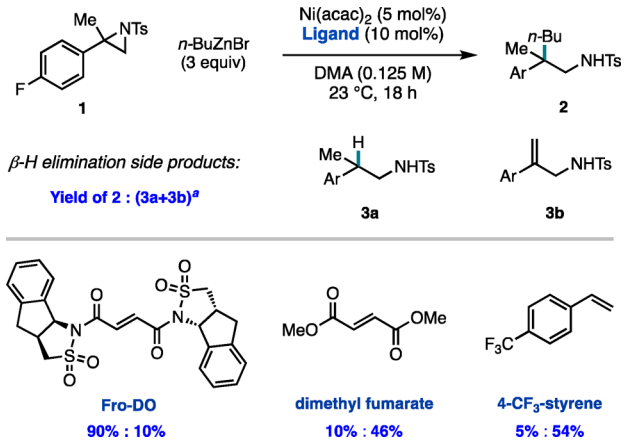

[a]^{19}F NMR yields.

reaction represents a rare example of a Ni-catalyzed Csp^3–Csp^3 cross-coupling reaction that forms quaternary carbon centers.[14−16] Under the optimized reaction conditions, cross-coupled product **2** is generated in high yields and high product selectivity over β-hydride elimination products **3a** and **3b**. Notably, dimethyl fumarate and 4-CF_3-styrene afforded mostly β-hydride elimination side products **3a** and **3b** despite their success as ligands for other Csp^3–Csp^3 cross-coupling reactions. Furthermore, reactions run in the absence of ligand or with other ligand classes delivered no desired cross-coupled product.

Motivated by the efficiency of this reaction system for quaternary carbon C–C bond formation and the unexplained difference in reaction outcome between Fro-DO and the other π-deficient ligands, we undertook a detailed investigation of the aziridine cross-coupling reaction. Here, we describe kinetic, spectroscopic, and computational studies aimed at elucidating its mechanism and the structural features of EDOs responsible for reactivity and selectivity. We present evidence that a Fro-DO-bound Ni^{II} azametallacyclobutane is the resting state of the catalyst and that Fro-DO-promoted Csp^3–Csp^3 reductive elimination is the turnover-limiting step. On the basis of computational studies and structure–activity relationships, we find that the feature that distinguishes Fro-DO from other olefinic ligands is its ability to coordinate favorably to Ni^{II} intermediates via its sulfonyl group. This surprising insight enabled us to redesign the ligand framework, resulting in a more synthetically accessible and modular ligand class, one member of which affords comparable activity to Fro-DO. This study affords a mechanistic platform for future ligand design efforts and has resulted in the discovery of a ligand framework that may prove of broad utility in the development of other challenging Ni-catalyzed Csp^3–Csp^3 cross-coupling reactions.

RESULTS AND DISCUSSION

Kinetic Analysis. At the outset of this study we considered two possible catalytic pathways for the reaction, following either a $Ni^{0/II}$ cycle or a $Ni^{I/III}$ cycle (Scheme 2). While $Ni^{0/II}$ cycles have been proposed for most aziridine cross-coupling reactions,[17] a $Ni^{I/III}$ catalytic cycle is commonly invoked for difficult alkyl–alkyl cross-coupling reactions since reductive elimination proceeds at a faster rate from Ni^{III} than from Ni^{II}.[18,19] Moreover, β-hydride elimination from a Ni^{I}-alkyl intermediate is expected to be less favorable than from a more electrophilic Ni^{II} center. To interrogate these possibilities kinetically, the Negishi cross-coupling of fluorinated aziridine **1** with *n*-BuZnBr was chosen as the model system (Scheme 1). We used a combination of Reaction Progress Kinetic Analysis (RPKA),[20] Burés' method of kinetic analysis,[21] initial rate kinetics, and Method of Continuous Variation (MCV)[22] to study the effect of reaction component concentrations on the rate of the catalytic reaction. All reactions were monitored using *in situ* ^{19}F NMR.

https://dx.doi.org/10.1021/jacs.0c02237
J. Am. Chem. Soc. 2020, 142, 8928−8937

Scheme 2. Possible Catalytic Cycles for the Ni-Catalyzed Csp^3–Csp^3 Cross-Coupling Reaction

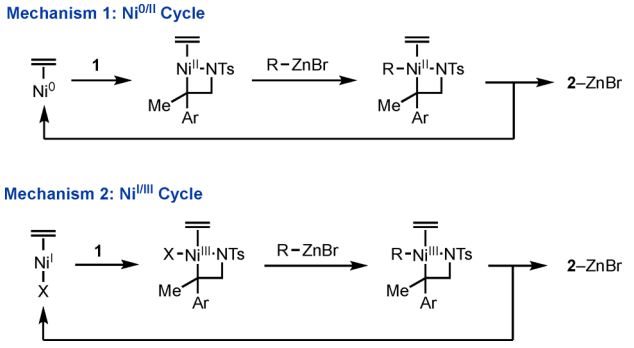

Catalyst Decomposition vs Product Inhibition. We began with the same excess protocol of RPKA, a useful tool to interrogate catalyst decomposition. We monitored two catalytic reactions, the standard reaction with an aziridine **1** concentration of 0.125 M and a same excess reaction at approximately 50% conversion ($[\mathbf{1}]_0$ = 0.065 M). As shown in Figure 2A, the rate profile of the same excess reaction did not overlay with that for the standard reaction. Instead, the standard reaction proceeded at a slower rate, indicating either catalyst deactivation or product inhibition. To probe these possibilities, we added product **2** (0.060 M) into the same excess reaction.[23] The resulting rate profile overlaid with the standard reaction, indicative of product inhibition. Product inhibition was further evaluated using the different excess protocol of RPKA in which the concentration of one reaction component is varied. While evaluating the reaction rates at aziridine concentrations in the range 0.065–0.125 M [**1**], an inverse first-order dependence on $[\mathbf{1}]_0$ was observed (Figure 2B). This unexpected observation can be rationalized based on the graphical rate law (Figure 2C). According to the identity shown in eq 3, the concentration of [**2**] is a function of $[\mathbf{1}]_0$ and [**1**]. Therefore, the apparent inverse first-order dependence on $[\mathbf{1}]_0$ is likely a result of an inverse first-order dependence on [**2**]. This is in agreement with the product inhibition result observed in the same excess experiment. Taken together, these data establish that minimal to no catalyst decomposition occurs over the course of the catalytic reaction.[24]

Kinetic Rate Orders. Additional different-excess experiments were performed to evaluate each reaction component and to determine the rate orders in [Ni], [Fro-DO], and [*n*-BuZnBr]. Variation of the Ni concentration from 4 to 11 mM (3–9 mol % loading), while maintaining the ligand concentration constant at 12.5 mM, revealed a first-order dependence on [Ni] (Figure 2E).[25,26] To determine the rate order in [Fro-DO], the concentration of Fro-DO was varied from 4 to 20 mM at constant Ni concentration. We observed saturation kinetic behavior in [Fro-DO] (Figure 2F).[27] Saturation kinetics was also observed for the rate dependence on [*n*-BuZnBr] (Figure 2G). At synthetically relevant conditions, [Fro-DO] = 12.5 mM and [*n*-BuZnBr] = 0.35 M, the reaction is zero-order in [Fro-DO] and first-order in [*n*-BuZnBr] suggesting that the catalyst resting state is ligand-bound and transmetalation occurs after formation of the catalyst resting state.

Product inhibition and the lack of an NMR handle on the organozinc reagent made obtaining a rate dependence on [**1**] using RPKA difficult. Therefore, we pursued the method of initial rates by monitoring the first 10% conversion of aziridine **1**. As shown in Figure 2D, we observed a zero-order dependence on $[\mathbf{1}]_0$. The lack of rate dependence on [**1**] demonstrates that the catalyst resting state of the reaction is an aziridine-bound Ni complex. Thus, oxidative addition can be ruled out as the turnover-limiting step of the reaction.

Ni:Fro-DO Stoichiometry. Although our previously reported catalytic conditions were optimized to a 1:2 ratio of metal to ligand, the Ni to Fro-DO stoichiometry at the transition state was determined to be 1:1 ($\chi_{\text{Fro-DO}}$ = 0.5, Figure 2H). Taken

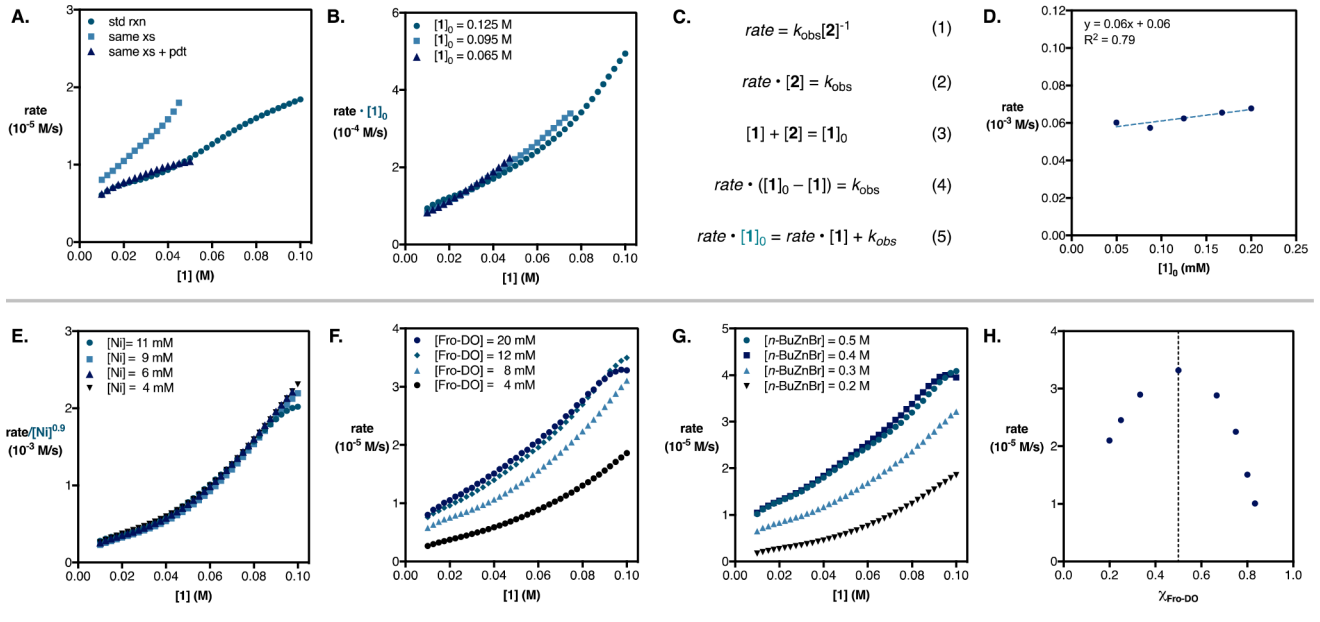

Figure 2. (A) Same excess experiments. (B) Different excess experiments varying $[\mathbf{1}]_0$. (C) Proposed graphical rate law for product inhibition. (D) Initial rates kinetic analysis on [**1**]. Different excess experiments varying (E) [Ni], (F) [Fro-DO], (G) [*n*-BuZnBr]. (H) MCV plot at various mole fractions of Fro-DO. $\chi_{\text{Fro-DO}} = \frac{\text{moles of Fro-DO}}{\text{fixed total moles of Fro-DO + Ni}}$.

https://dx.doi.org/10.1021/jacs.0c02237
J. Am. Chem. Soc. 2020, 142, 8928–8937

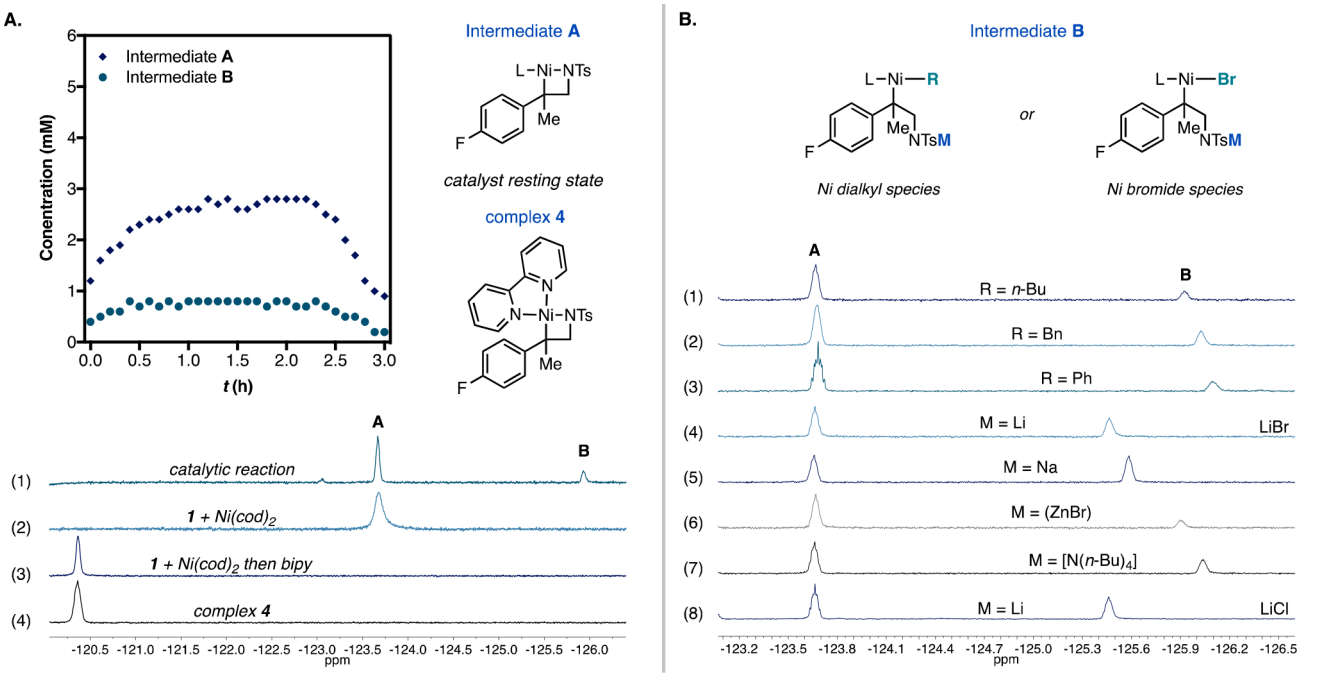

Figure 3. ^{19}F NMR studies (solvent = DMA). (A) Observation of Ni catalytic intermediates and structure determination of Ni intermediate **A**. (B) Structure determination of Ni intermediate **B**.

together with the first-order kinetic dependence on [Ni] and zero-order dependence on [Fro-DO], these results suggest that there is only one molecule of Fro-DO bound to Ni throughout the catalytic cycle.

Spectroscopic Analysis. We turned to spectroscopic studies to further interrogate the mechanism of the reaction. ^{19}F NMR studies of the catalytic reaction showed the appearance of two peaks (δ) at −123.7 ppm (**A**) and −125.9 ppm (**B**), which both disappear at the end of the reaction or upon exposure to air. The air sensitivity of these two species is suggestive of Ni intermediates. No significant changes were observed in the concentration of these two intermediates over the course of reaction, indicating that if these two species are catalytic intermediates, steady-state kinetics are achieved and no change in mechanism takes place (Figure 3A).

*Ni Intermediate **A**.* The addition of aziridine **1** to Ni(cod)$_2$ (0.5 equiv) in DMA at room temperature causes a gradual color change from yellow to red over the course of 20 min, with generation of the peak **A** observed in the catalytic reaction (Figure 3A, spectrum 2). UV−vis spectroscopic analysis of the red aziridine **1**/Ni(cod)$_2$ mixture showed an absorption band at 505 nm (λ_{max}) consistent with a d-d transition of a Ni^{II} d^8-complex.[28] The assignment of a Ni^{II} oxidation state was supported by electron paramagnetic resonance (EPR) studies of the catalytic reaction mixture, which showed no Ni^{I} or Ni^{III} species (Figure S16). The newly formed Ni complex proved difficult to isolate and decomposed in solution after 20 min. The unstable complex could, however, be stabilized by addition and trapping with bipyridine, causing the peak at −123.7 ppm to disappear and a new peak at −120.3 ppm to appear (spectrum 3). The new species was assigned as azametallacyclobutane complex **4** by independent preparation and NMR characterization of **4** from (bipy)NiEt$_2$ and **1** according to the procedure from Hillhouse (spectrum 4).[29] With this structural assignment, the concentration of intermediate **A** in the catalytic reaction was calculated using an internal standard to be approximately 50% of the total Ni concentration; **A** is thus the catalyst resting state. This observation is consistent with the zero-order rate dependence on [**1**]. Furthermore, this experiment provides evidence that an olefinic ligand is not required for the oxidative addition step.[30] The peak for the *in situ* generated oxidative adduct (spectrum 2) overlaps with that of intermediate **A** in the catalytic reaction. ^{19}F NMR is inconclusive, however, in determining the ligation state of Ni intermediate **A**. Based on the observation of zero-order kinetic dependence on [Fro-DO] and further support by DFT,[31] we propose that intermediate **A** is the Fro-DO-bound Ni oxidative adduct.

*Ni Intermediate **B**.* Having assigned intermediate **A** as the Ni oxidative adduct of aziridine **1**, we proceeded to investigate the minor peak at −125.9 ppm (**B**). As with intermediate **A**, the absence of EPR signals associated with the catalytic reaction mixture argued against a Ni^{I} or Ni^{III} oxidation state. Initially we considered two possible structures for intermediate **B** that would result from the reaction of intermediate **A** with *n*-BuZnBr. One possibility is a Ni^{II}-dialkyl species resulting from transmetalation of intermediate **A** with *n*-BuZnBr (Figure 3B). Alternatively, intermediate **B** could be a Ni^{II}-bromide species arising from ring opening of intermediate **A** by a bromide ion. To interrogate these two possibilities, we performed spectroscopic experiments with distinct organozinc reagents. By changing the organozinc reagent in the catalytic reaction from *n*-BuZnBr to BnZnBr and PhZnBr,[32] we observed distinguishable changes in the chemical shift of intermediate **B**, providing evidence for a Ni^{II}-dialkyl intermediate (Figure 3B, spectra 1−3). Next, we probed the proposed anionic nature of the sulfonamide group of Ni intermediate **B**. Various bromide salts (0.4 equiv) were added to the catalytic reaction, and the effect on the chemical shift of intermediate **B** was evaluated. Indeed, the chemical shift of intermediate **B** was sensitive to the identity of the cations (M$^+$) in solution in a

https://dx.doi.org/10.1021/jacs.0c02237
J. Am. Chem. Soc. 2020, 142, 8928−8937

manner that is consistent with the expected cation Lewis acidity ($Li^+ > Na^+ > Zn^{2+} > [N(n\text{-}Bu)_4]^+$) (spectra 4−7). Finally, consistent with the assignment of intermediate **B** as the Ni^{II}-dialkyl species, the chemical shift of **B** remained invariant whether LiBr or LiCl (0.4 equiv) was added to the catalytic reaction (spectra 4 and 8).

Proposed Catalytic Cycle. The kinetic and spectroscopic evidence presented above is inconsistent with a $Ni^{I/III}$ catalytic cycle. First, no $Ni^{I/III}$ species were observed in the reaction mixture by EPR. Second, Ni^{II} intermediate **A**, whose structure was supported by trapping as **4**, is formed and consumed under the catalytic conditions and accounts for the resting state of the catalyst (Figure 3). Thus, we propose a $Ni^{0/II}$ catalytic cycle, initiated by reduction of $Ni(acac)_2$ by the organozinc reagent to form Ni^0 which undergoes rapid oxidative addition to aziridine **1** to form the azametallacyclobutane intermediate (Scheme 3).[33] The observed saturation kinetic dependence on

Scheme 3. Proposed Catalytic Cycle Based on Kinetic and Spectroscopic Data (M = ZnBr)

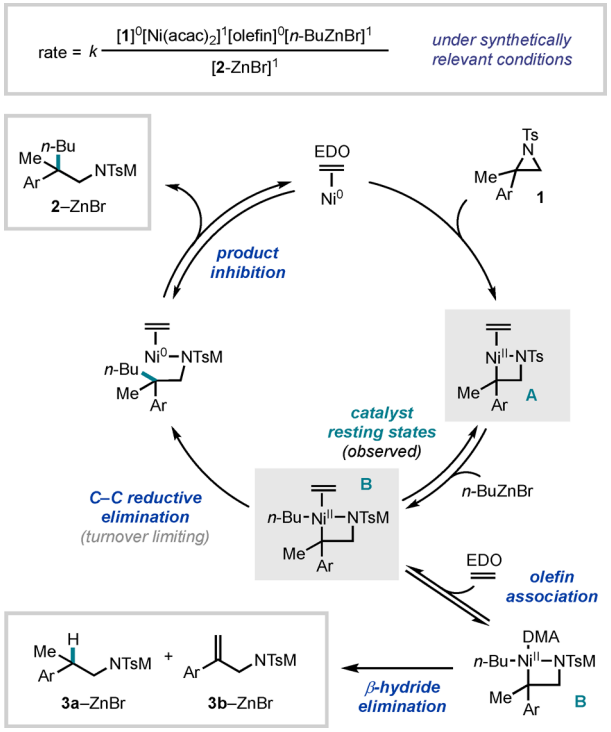

Fro-DO indicates that association of Fro-DO to the Ni^{II} oxidative adduct is fast and reversible favoring ligated Ni intermediate **A** under synthetically relevant conditions. The olefin-bound oxidative adduct **A** undergoes transmetalation with *n*-BuZnBr to afford intermediate **B**, both of which were observed spectroscopically under the reaction conditions (**A**:**B** ≈ 3.5:1).[34] While the first-order dependence on organozinc could support a turnover-limiting transmetalation, we discount this possibility based on the observation of post-transmetalation intermediate **B**. Thus, the data support a turnover-limiting reductive elimination from intermediate **B** to provide cross-coupled product **2**−ZnBr bound to a regenerated Ni^0. Ni sequestered by product **2** accounts for the product inhibition observed in the reaction.[24b] Based on the spectroscopic evidence for oxidative adduct **A** and Ni^{II}-dialkyl intermediate **B**, as well as the rate orders for all reaction components, we conclude that the turnover-limiting step of the catalytic cycle is reductive elimination. Turnover-limiting reductive elimination is consistent with difficult Csp^3−Csp^3 bond formation, especially one involving formation of a quaternary carbon.

Elucidation of Ligand Effects. With experimental evidence establishing turnover-limiting C−C reductive elimination from an olefin-bound Ni^{II}-dialkyl intermediate, we turned to Density Functional Theory (DFT) to probe the impact that different EDO ligands have on C−C reductive elimination and association to Ni^{II}-dialkyl intermediate **B**. Two simplifications were performed in our DFT studies on the Ni^{II}-dialkyl intermediate: (1) a phenyl group was used instead of the 4-fluorophenyl group of aziridine **1** and (2) a neutral sulfonamide group was modeled instead of the anionic sulfonamide group.[35] DFT calculations were performed using a combination of B3LYP/6-31G(d,p) for geometry optimizations and frequency calculations and M06/6-311+G(d,p) for single-point energy calculations. Two additional olefins were included in the DFT analysis in order to elucidate trends: 1-hexene and fumaronitrile were chosen because they span a wide range of electron deficiency based on LUMO energies.

C−C Reductive Elimination Activation Barrier. We began our DFT analysis by evaluating the effect of the various olefinic ligands on the turnover-limiting C−C reductive elimination step. Engle and co-workers computationally compared Csp^2−Csp^3 reductive elimination from Ni^{II} for dimethyl fumarate, ethylene, and solvent-bound Ni intermediates.[12] To our knowledge, however, an evaluation of structurally differentiated EDOs and their influence on Csp^3−Csp^3 reductive elimination from Ni^{II} has not been performed.[12,36] Transition state structures were computed for the various electronically differentiated olefin-bound Ni^{II}-dialkyl intermediates and used to obtain activation barriers ($\Delta G^{\ddagger}$). As shown in Figure 4A, the highest computed C−C reductive elimination barrier is for the 1-hexene-bound Ni intermediate ($\Delta G^{\ddagger}$ = 34.4 kcal/mol). 4-CF_3-Styrene affords a 4.2 kcal/mol reduction in the activation barrier ($\Delta G^{\ddagger}$ = 30.2 kcal/mol), consistent with the ability of π-deficient olefins to lower the barrier of reductive elimination, though in this case, not to a large enough degree to enable a synthetically feasible reaction at room temperature. For Fro-DO- and dimethyl fumarate-bound Ni intermediates, the barriers are lowered substantially to 23.0 and 23.4 kcal/mol, respectively. Fumaronitrile exhibits an activation barrier of 14.4 kcal/mol, but under experimental conditions this ligand is subject to decomposition pathways that make it intractable. Notably, C−C reductive elimination activation barriers appear to be largely governed by the electronic properties of the olefin, as illustrated by the correlation between the LUMO energy and activation barrier shown in Figure 4A. On this basis alone, DFT predicts that Fro-DO and dimethyl fumarate should be of comparable activity since the two ligands have similar LUMO energies (Figure 4B). However, this is inconsistent with the disparate yields observed in the catalytic reaction.

Olefin Association. Alternatively, we considered that olefin association to the Ni^{II}-dialkyl intermediate may give rise to the differences in reaction outcome. Tolman has previously investigated the association of olefinic ligands to Ni experimentally and found that log(K) correlates with olefin E_{LUMO}.[37] While this would not be expected to differentiate Fro-DO from dimethyl fumarate given the similarity in their E_{LUMO} energies, these studies were conducted with Ni^0 and a similar

https://dx.doi.org/10.1021/jacs.0c02237
J. Am. Chem. Soc. 2020, 142, 8928−8937

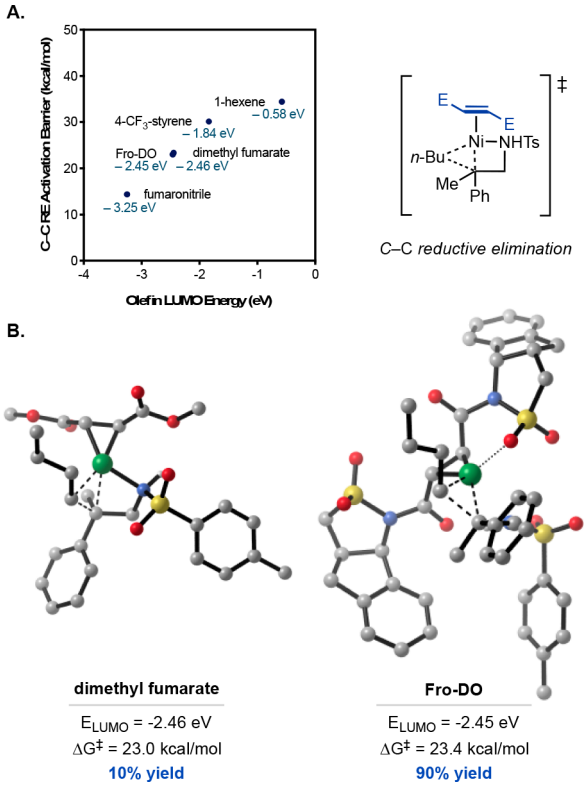

Figure 4. (A) C−C reductive elimination activation barriers vs olefin LUMO energy (computed at the M06 level of theory). (B) π-Backbonding and reductive elimination barriers do not explain the differential performance of dimethyl fumarate and Fro-DO.

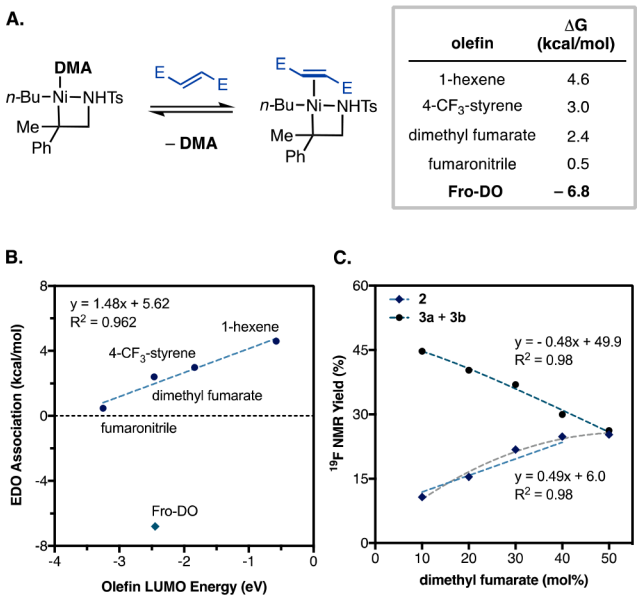

Figure 5. (A) Free energies change (ΔG) for olefin association to a Ni^{II}-dialkyl intermediate, corrected to account for concentrations under synthetically relevant conditions. (B) Plot of ΔG vs olefin E_{LUMO}. (C) Product distribution at different loadings of dimethyl fumarate.

investigation has not been conducted with Ni^{II}. Thus, we continued the head-to-head comparison between the olefinic ligands by evaluating their association behavior to Ni^{II}. More specifically, the Gibbs free-energy changes (ΔG) for olefin association to the solvent-bound Ni intermediate **B** were computed and are shown in Figure 5A−B. These values are corrected to account for the concentrations of all species under synthetically relevant conditions (see Supporting Information). Similar to the trend observed by Tolman and for the C−C reductive elimination activation barriers in Figure 4A, olefin association to the Ni^{II}-dialkyl intermediate was found to correlate with LUMO energies of the free olefin. Binding of the simple olefinic ligands exhibits ΔG values ranging from 4.6 kcal/mol for 1-hexene to 0.5 kcal/mol for fumaronitrile. However, Fro-DO does not follow the expected trend and DFT predicts a large negative free-energy change for its association (ΔG = −6.8 kcal/mol), favoring the olefin-bound Ni intermediate.[38] These results identify the difference between Fro-DO and dimethyl fumarate as originating from its ability to coordinate favorably to the Ni^{II}-dialkyl intermediate **B** by approximately 9 kcal/mol.

The observed selectivity for cross-coupled product vs β-hydride elimination side products can be understood from Figure 6, which depicts the overall energy landscape. Regardless of what EDO is present, the β-hydride elimination side products **3a** and **3b** are envisioned to form via the same coordinatively unsaturated Ni intermediate. This intermediate can undergo β-hydride elimination with the *n*-Bu group followed by C−H reductive elimination to form side product **3a′** ($\Delta G^{‡}$ = 17.1 kcal/mol (Figures 6, S32). Alternatively, the unsaturated Ni intermediate can undergo β-hydride elimination with the aziridine-derived methyl group, generating side product **3b′** ($\Delta G^{‡}$ = 19.7 kcal/mol). The relative barriers of β-hydride elimination and C−C reductive elimination are consistent with the fact that Fro-DO provides predominantly desired product while dimethyl fumarate provides predominantly undesired β-hydride elimination products. As discussed above, this distinction arises from Fro-DO's stronger association to intermediate **B**, rather than a lower barrier for reductive elimination.

To experimentally evaluate these DFT studies, we posited that it should be possible to improve product selectivity with dimethyl fumarate simply by increasing its concentration to favor the olefin-bound Ni intermediate since the ligand is predicted by DFT to substantially reduce the barrier to C−C reductive elimination ($\Delta G^{‡}$ = 23.0 kcal/mol). In contrast, the computational analysis suggests that 4-CF_3-styrene should not be a competent ligand ($\Delta G^{‡}$ = 30.2 kcal/mol), independent of its concentration. Thus, we evaluated the yield of cross-coupled product **2** and β-hydride elimination products **3a** and **3b** at higher loadings of both dimethyl fumarate and 4-CF_3-styrene. As the loading of dimethyl fumarate was increased from 10−50 mol %, we observed an increase in yield of cross-coupled product **2** accompanied by an equal decrease in the yields of β-hydride elimination products **3a** and **3b** (Figure 5C). At approximately 50 mol % loading, the catalytic reaction is saturated in dimethyl fumarate ultimately achieving a 1:1 selectivity of cross-coupled to combined β-hydride elimination products.[39] Use of 4-CF_3-styrene however led to full conversion of starting material without any appreciable yield of cross-coupled product **2** (<5% ^{19}F NMR yield) even at 100 mol % loading. These experimental results provide support for the DFT analysis and indicate that the primary difference between Fro-DO and dimethyl fumarate originates in association to Ni^{II}.

Ni:Fro-DO Interactions. The binding of the simple olefins to the Ni^{II}-dialkyl intermediate is largely dictated by Ni π-

https://dx.doi.org/10.1021/jacs.0c02237
J. Am. Chem. Soc. 2020, 142, 8928−8937

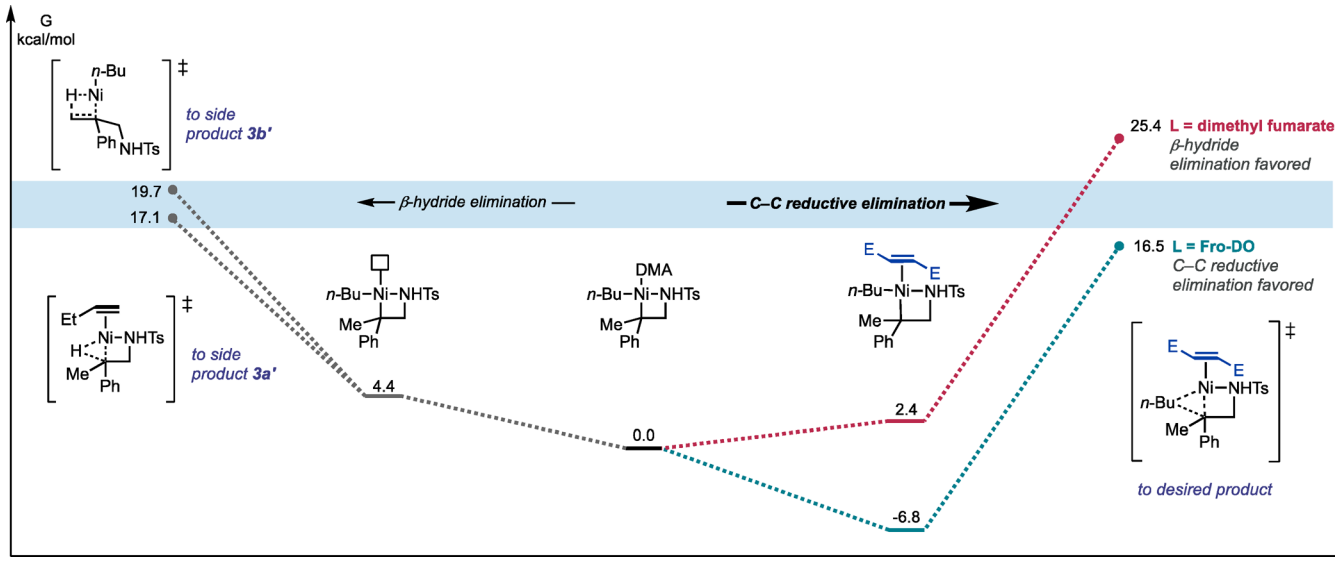

Figure 6. Energy landscape for formation of desired C−C reductive elimination products and undesired β-hydride elimination products. **3a′** and **3b′** refer to the desfluoro versions of **3a** and **3b**. The barrier shown leading to **3a′** is for the C−H reductive elimination following β-hydride elimination of the *n*-Bu group (see Figure S32).

backbonding interactions as described by the Dewar−Chatt−Duncanson model.[40] Strong Ni−olefin bonds are observed with π-deficient olefins characterized by low-lying LUMO energies. Fro-DO's association to Ni, however, is not solely governed by Ni π-backbonding since Fro-DO and dimethyl fumarate have similar LUMO energies, yet Fro-DO exhibits olefin association behavior that is approximately 9 kcal/mol lower in energy. A closer look at the computed geometry of the Fro-DO-bound Ni^{II} intermediate reveals a potential explanation for the unexpected favorability of Fro-DO association. One of Fro-DO's sulfonyl groups is in close proximity to Ni (Ni−O = 2.40 Å) resembling an axial ancillary ligand for the square-planar complex (Figure 7). In order to probe this

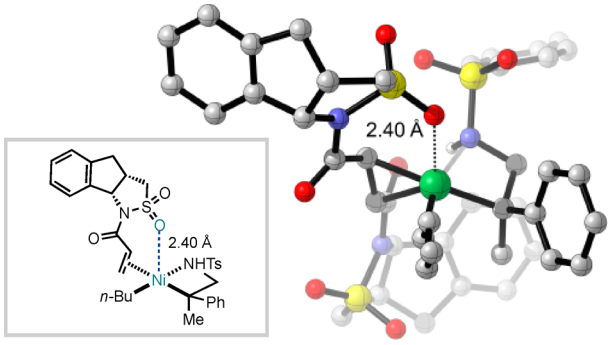

Figure 7. Ground state structure of the Fro-DO-bound Ni^{II}-dialkyl intermediate. Only half of Fro-DO is shown in the inset.

interaction, we performed a second-order perturbation theory analysis as carried out in a Natural Bond Order (NBO) calculation.[41] Indeed we found a donor/acceptor interaction between one of the sulfonyl oxygen lone pairs and an empty p-orbital on Ni with a computed $E(2)$ delocalization energy of 12.3 kcal/mol.[42]

Linear Regression Analysis. Based on the second-order perturbation theory analysis of the Fro-DO-bound Ni^{II} intermediate, coordination of Fro-DO's sulfonyl group to Ni^{II} provides a highly stabilizing secondary interaction. We therefore set out to interrogate this effect experimentally through the use of structure−activity relationships. We envisioned modifying Fro-DO's structure by replacing the methylene proximal to the sulfonyl group with a N−R group (Figure 8A). This modification to the ligand framework would allow the facile installment of a variety of *N*-substituents that we expected would impact the Lewis basicity of the sulfonyl group while having minimal influence on the olefin LUMO energy.

Data Collection. A simple three-step sequence (see Supporting Information Section X) afforded 9 new ligands with sterically and electronically differentiated alkyl, benzyl, and aryl groups at the sulfonamide nitrogen. The new ligands were tested in the aziridine cross-coupling reaction and found to exhibit large reactivity differences with a range in the yield of **2** from 11% (R = Me) to 72% (R = Cyp). One of the ligands bearing a highly electron-deficient group (R = 4-CF_3-Ph) failed to provide any appreciable yield of **2** (<5% ^{19}F NMR yield). Geometry optimized structures for the olefin-bound Ni^{II} intermediates were then obtained by DFT for each of the synthesized ligands in the set. This was followed by an NBO second-order perturbation theory analysis to obtain the sulfonyl oxygen−Ni interaction stabilization energy. The delocalization energies and the Ni−O distances are shown in Figure 8B. Since the delocalization energy largely depends on how far apart the two interacting species are, a linear correlation was observed between $E(2)$ and the Ni−O distance (R^2 = 0.98). For comparison, E_{LUMO} of the free ligands were also computed.

Linear Regression. Modeling the 8 new ligands that delivered cross-coupled product **2** and Fro-DO led to the positive univariate linear correlation between the computed $E(2)$ and the yield of **2** (R^2 = 0.80, Figure 8C). Highly stabilizing secondary interactions arising from electron-rich sulfonyl groups trend with high yields of cross-coupled product as expected from the DFT-derived hypothesis but counter-intuitive according to the traditional view of the role of EDOs (more electron deficient is more effective). On the other hand, a poor correlation was observed (R^2 = 0.26) between the yield

https://dx.doi.org/10.1021/jacs.0c02237
J. Am. Chem. Soc. 2020, 142, 8928−8937

A.

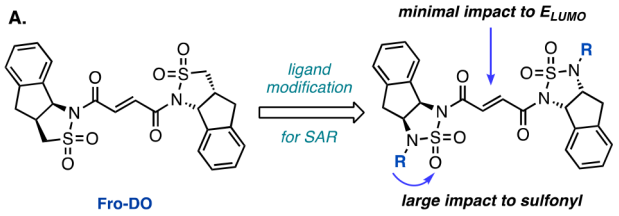

B.

R	Yield of 2 (%)	Ni–O (Å)	E(2) (kcal)	E_{LUMO} (eV)
Me	11	2.52	8.72	− 2.48
i-Pr	72	2.36	11.81	− 2.40
Cyp	72	2.38	11.29	− 2.38
Ph	46	2.43	10.16	− 2.45
4-CF_3-Ph	< 5	3.21	1.94	− 2.73
Bn	50	2.36	11.79	− 2.46
4-F-Bn	51	2.41	10.71	− 2.56
4-CF_3-Bn	36	2.41	10.67	− 2.68
4-OMe-Bn	59	2.38	11.31	− 2.40
Fro-DO	81	2.40	12.27	− 2.45

C.

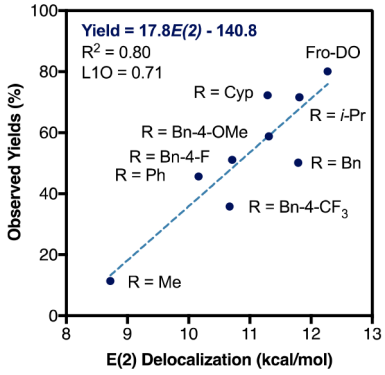

Figure 8. (A) Redesigned ligand framework to interrogate the structural basis for reactivity. (B) Impact of ligand structure on the yield of **2** (conditions as noted in Scheme 1) and corresponding calculated Ni–O bond distance, $E(2)$, and E_{LUMO}. (C) Linear regression analysis.

of **2** and the olefin LUMO energies consistent with our hypothesis. The 4-CF_3-phenyl ligand was not included in the model, since we expect that any product formation arises from a background reaction. Nevertheless, the computed $E(2)$ value of 1.9 kcal/mol agrees with the hypothesis that a ligand lacking this stabilizing secondary interaction fails to deliver cross-coupled product despite having a LUMO energy that is lower than that of Fro-DO.

CONCLUSION

We have performed a mechanistic investigation of a Ni-catalyzed cross-coupling reaction of 2,2-disubstituted aziridines requiring the use of an EDO ligand. A series of kinetic and spectroscopic analyses provide evidence for turnover-limiting C–C reductive elimination within a $Ni^{0/II}$ cycle, consistent with difficult Csp^3–Csp^3 bond formation involving a 3°-carbon coupling partner. Computational and experimental studies shed light on why Fro-DO shows unique reactivity for C–C bond formation compared to other olefin ligands previously investigated for Ni-catalyzed cross couplings. Whereas Fro-DO and dimethyl fumarate both lower the barrier to C–C reductive elimination due to their low-lying LUMO energies, only Fro-DO binds favorably to Ni^{II} based on a combination of strong Ni π-backbonding and a secondary interaction between the ligand's sulfonyl group and Ni^{II}. Structure–activity relationships within a new EDO-ligand framework provide experimental evidence of this secondary Ni–olefin interaction. This insight thus lays a path for mechanism-driven improvement of catalytic activity and applications of the ligand class to other challenging cross-coupling reactions.

ASSOCIATED CONTENT

Supporting Information

The Supporting Information is available free of charge at https://pubs.acs.org/doi/10.1021/jacs.0c02237.

X-ray crystal structure of **L2** R = *i*-Pr Ligand (CIF)

Experimental procedures, computational data, and characterization and spectral data for new compounds (PDF)

AUTHOR INFORMATION

Corresponding Author

Abigail G. Doyle − *Department of Chemistry, Princeton University, Princeton, New Jersey 08544, United States;* orcid.org/0000-0002-6641-0833; Email: agdoyle@princeton.edu

Authors

Jesús G. Estrada − *Department of Chemistry, Princeton University, Princeton, New Jersey 08544, United States;* orcid.org/0000-0001-9578-6912

Wendy L. Williams − *Department of Chemistry, Princeton University, Princeton, New Jersey 08544, United States;* orcid.org/0000-0003-2227-0856

Stephen I. Ting − *Department of Chemistry, Princeton University, Princeton, New Jersey 08544, United States;* orcid.org/0000-0002-6146-8112

Complete contact information is available at: https://pubs.acs.org/10.1021/jacs.0c02237

Notes

The authors declare no competing financial interest.

ACKNOWLEDGMENTS

Dedicated to Professor Eric N. Jacobsen on the occasion of his 60th birthday. The authors gratefully acknowledge Dr. Dennis C.-Y. Huang and Sonya Karchesmkiy for helpful advice; Professor Matthew Sigman for guidance on performing multivariate linear regression; Dr. István Pelczer and Kenith Conover for NMR assistance; and Phillip Jeffrey for obtaining an X-ray crystal structure. Financial support was provided by NIGMS (R35 GM126986).

REFERENCES

(1) Johansson Seechurn, C.; Kitching, M.; Colacot, T.; Snieckus, V. Palladium-Catalyzed Cross-Coupling: A Historical Contextual Perspective to the 2010 Nobel Prize. *Angew. Chem., Int. Ed.* **2012**, *51*, 5062–5085.

(2) For a general review on advances in Ni catalysis, see: (a) Tasker, S. Z.; Standley, E. A.; Jamison, T. F. Recent Advances in Homogeneous Nickel Catalysis. *Nature* **2014**, *509*, 299. For reviews on sp^3-couplings, see: (b) Choi, J.; Fu, G. Transition Metal-Catalyzed Alkyl-Alkyl bond formation: Another Dimension in Cross-Coupling chemistry. *Science* **2017**, *356*, No. eaaf7230. (c) Fu, G. Transition-Metal Catalysis of Nucleophilic Substitution Reactions: A Radical

Alternative to S_N1 and S_N2 Processes. *ACS Cent. Sci.* **2017**, *3*, 692−700.
(3) Low, J. J.; Goddard, W. A., III Theoretical Studies of Oxidative Addition and Reductive Elimination. 2. Reductive Coupling of H−H, H−C, and C−C Bonds from Palladium and Platinum Complexes. *Organometallics* **1986**, *5*, 609−622.
(4) Johnson, J.; Rovis, T. More than Bystanders: The Effect of Olefins on Transition-Metal-Catalyzed Cross-Coupling Reactions. *Angew. Chem., Int. Ed.* **2008**, *47*, 840−871.
(5) Lau, J.; Sustmann, R. Diethyl-2,2′-Bipyridyl-Palladium(II), a Case for the Study of Combination vs. Disproportionation Products. *Tetrahedron Lett.* **1985**, *26*, 4907−4910.
(6) Tatsumi, K.; Nakamura, A.; Komiya, S.; Yamamoto, A.; Yamamoto, T. An Associative Mechanism for Reductive Elimination of d^8 $NiR_2(PR_3)_2$. *J. Am. Chem. Soc.* **1984**, *106*, 8181−8188.
(7) Tatsumi, K.; Hoffmann, R.; Yamamoto, A.; Stille, J. K. Reductive Elimination of d^8-Organotransition Metal Complexes. *Bull. Chem. Soc. Jpn.* **1981**, *54*, 1857−1867.
(8) (a) Giovannini, R.; Knochel, P. Ni(II)-Catalyzed Cross-Coupling between Polyfunctional Arylzinc Derivatives and Primary Alkyl Iodides. *J. Am. Chem. Soc.* **1998**, *120*, 11186−11187. (b) Jensen, A.; Knochel, P. Nickel-Catalyzed Cross-Coupling between Functionalized Primary or Secondary Alkylzinc Halides and Primary Alkyl Halides. *J. Org. Chem.* **2002**, *67*, 79−85. (c) Piber, M.; Jensen, A.; Rottländer, M.; Knochel, P. New Efficient Nickel- and Palladium-Catalyzed Cross-Coupling Reactions Mediated by Tetrabutylammonium Iodide. *Org. Lett.* **1999**, *1*, 1323−1326. (d) Giovannini, R.; Stüdemann, T.; Devasagayaraj, A.; Dussin, G.; Knochel, P. New Efficient Nickel-Catalyzed Cross-Coupling Reaction between Two Csp^3 Centers. *J. Org. Chem.* **1999**, *64*, 3544−3553.
(9) Rovis and co-workers evaluated similar ligands for Ni-catalyzed Negishi Csp^2−Csp^3 cross-coupling of cyclic anhydrides. (a) Bercot, E.; Rovis, T. A Mild and Efficient Catalytic Alkylative Monofunctionalization of Cyclic Anhydrides. *J. Am. Chem. Soc.* **2002**, *124*, 174−175. (b) Johnson, J.; Bercot, E.; Rowley, J.; Coates, G.; Rovis, T. Ligand-Dependent Catalytic Cycle and Role of Styrene in Nickel-Catalyzed Anhydride Cross-Coupling: Evidence for Turnover-Limiting Reductive Elimination. *J. Am. Chem. Soc.* **2007**, *129*, 2718−2725.
(10) For other examples of using EDO ligands to improve product selectivity in Pd catalysis, see: (a) Luo, X.; Zhang, H.; Duan, H.; Liu, Q.; Zhu, L.; Zhang, T.; Lei, A. Superior Effect of a π-Acceptor Ligand (Phosphine-Electron-Deficient Olefin Ligand) in the Negishi Coupling Involving Alkylzinc Reagents. *Org. Lett.* **2007**, *9*, 4571−4574. (b) Zhang, H.; Luo, X.; Wongkhan, K.; Duan, H.; Li, Q.; Zhu, L.; Wang, J.; Batsanov, A.; Howard, J. K.; Marder, T.; Lei, A. Acceleration of Reductive Elimination of [Ar-Pd-C_{sp^3}] by a Phosphine/Electron-Deficient Olefin Ligand: A Kinetic Investigation. *Chem. - Eur. J.* **2009**, *15*, 3823−3829. (c) Gioria, E.; Martínez-Ilarduya, J.; Espinet, P. Experimental Study of the Mechanism of the Palladium-Catalyzed Aryl-Alkyl Negishi Coupling Using Hybrid Phosphine-Electron-Withdrawing Olefin Ligands. *Organometallics* **2014**, *33*, 4394−4400.
(11) (a) Huang, C.-Y.; Doyle, A. G. Nickel-Catalyzed Negishi Alkylations of Styrenyl Aziridines. *J. Am. Chem. Soc.* **2012**, *134*, 9541−9544. (b) Nielsen, D. K.; Huang, C.-Y.; Doyle, A. G. Directed Nickel-Catalyzed Negishi Cross Coupling of Alkyl Aziridines. *J. Am. Chem. Soc.* **2013**, *135*, 13605−13609.
(12) The Engle group recently published a Ni catalyzed Csp^2−Csp^3 Suzuki cross-coupling method using dimethyl fumarate as a ligand. Derosa, J.; Kleinmans, R.; Tran, V.; Karunananda, M.; Wisniewski, S.; Eastgate, M.; Engle, K. Nickel-Catalyzed 1,2-Diarylation of Simple Alkenyl Amides. *J. Am. Chem. Soc.* **2018**, *140*, 17878−17883.
(13) Huang, C.-Y.; Doyle, A. G. Electron-Deficient Olefin Ligands Enable Generation of Quaternary Carbons by Ni-Catalyzed Cross-Coupling. *J. Am. Chem. Soc.* **2015**, *137*, 5638−5641.
(14) For examples of Ni-catalyzed Csp^3−Csp^2 quaternary carbon bond formations, see: (a) Ariki, Z.; Maekawa, Y.; Nambo, M.; Crudden, C. Preparation of Quaternary Centers via Nickel-Catalyzed Suzuki-Miyaura Cross-Coupling of Tertiary Sulfones. *J. Am. Chem. Soc.* **2018**, *140*, 78−81. (b) Zhou, Q.; Cobb, K. M.; Tan, T.; Watson, M. Stereospecific Cross Couplings to Set Benzylic, All-Carbon Quaternary Stereocenters in High Enantiopurity. *J. Am. Chem. Soc.* **2016**, *138*, 12057−12060. (c) Zultanski, S. L.; Fu, G. Nickel-Catalyzed Carbon-Carbon Bond-Forming Reactions of Unactivated Tertiary Alkyl Halides: Suzuki Arylations. *J. Am. Chem. Soc.* **2013**, *135*, 624−627. (d) Wang, X.; Wang, S.; Xue, W.; Gong, H. Nickel-Catalyzed Reductive Coupling of Aryl Bromides with Tertiary Alkyl Halides. *J. Am. Chem. Soc.* **2015**, *137*, 11562−11565. (e) Wang, X.; Ma, G.; Peng, Y.; Pitsch, C. E.; Moll, B. J.; Ly, T. D.; Wang, X.; Gong, H. Ni-Catalyzed Reductive Coupling of Electron-Rich Aryl Iodides with Tertiary Alkyl Halides. *J. Am. Chem. Soc.* **2018**, *140*, 14490−14497. (f) Primer, D. N.; Molander, G. A. Enabling the Cross-Coupling of Tertiary Organoboron Nucleophiles through Radical-Mediated Alkyl Transfer. *J. Am. Chem. Soc.* **2017**, *139*, 9847−9850. (g) Chen, T.-G.; Zhang, H.; Mykhailiuk, P. K.; Merchant, R. R.; Smith, C. A.; Qin, T.; Baran, P. S. Quaternary centers via Ni-catalyzed cross-coupling of tertiary carboxylic acids and aryl zinc reagents. *Angew. Chem., Int. Ed.* **2019**, *58*, 2454−2458.
(15) For examples of Ni-catalyzed Csp^3−Csp^3 quaternary carbon bond formation, see: (a) Green, S. A.; Huffman, T. R.; McCourt, R. O.; van der Puyl, V.; Shenvi, R. A. Hydroalkylation of Olefins to Form Quaternary Carbons. *J. Am. Chem. Soc.* **2019**, *141*, 7709−7714. (b) Qin, T.; Malins, L. R.; Edwards, J. T.; Merchant, R. R.; Novak, A. J. E.; Zhong, J. Z.; Mills, R. B.; Yan, M.; Yuan, C.; Eastgate, M. D.; Baran, P. S. Nickel-Catalyzed Barton Decarboxylation and Giese Reactions: A Practical Take on Classic Transforms. *Angew. Chem., Int. Ed.* **2017**, *56*, 260−265. (c) Ye, Y.; Chen, H.; Sessler, J. L.; Gong, H. Zn-Mediated Fragmentation of Tertiary Alkyl Oxalates Enabling Formation of Alkylated and Arylated Quaternary Carbon Centers. *J. Am. Chem. Soc.* **2019**, *141*, 820−824.
(16) DFT calculations indicate that C−C reductive elimination proceeds with a barrier higher by 10.9 kcal/mol when the aziridine is 2,2-disubstituted as opposed to 2-monosubstituted. See Figure S33.
(17) Jensen, K. L.; Standley, E. A.; Jamison, T. F. Highly Regioselective Nickel-Catalyzed Cross-Coupling of *N*-Tosylaziridines and Alkylzinc Reagents. *J. Am. Chem. Soc.* **2014**, *136*, 11145−11152.
(18) Zheng, B.; Tang, F.; Luo, J.; Schultz, J. W.; Rath, N.; Mirica, L. Organometallic Nickel(III) Complexes Relevant to Cross-Coupling and Carbon-Heteroatom Bond Formation Reactions. *J. Am. Chem. Soc.* **2014**, *136*, 6499−6504.
(19) Diccianni, J. B.; Diao, T. Mechanisms of Nickel-Catalyzed Cross-Coupling Reactions. *Trends in Chemistry* **2019**, *1*, 830−844.
(20) Blackmond, D. Kinetic Profiling of Catalytic Organic Reactions as a Mechanistic Tool. *J. Am. Chem. Soc.* **2015**, *137*, 10852−10866.
(21) Burés, J. A Simple Graphical Method to Determine the Order in Catalyst. *Angew. Chem., Int. Ed.* **2016**, *55*, 2028−2031.
(22) Renny, J.; Tomasevich, L.; Tallmadge, E.; Collum, D. Method of Continuous Variations: Applications of Job Plots to the Study of Molecular Associations in Organometallic Chemistry. *Angew. Chem., Int. Ed.* **2013**, *52*, 11998−12013.
(23) Product **2** was added as the zinc bromide salt (**2**-ZnBr) to mimic reaction conditions.
(24) (a) A series of NMR spectroscopic studies (see Section V of the Supporting Information) suggests that the mechanism of product inhibition is likely an equilibrium between Ni^0 and product. For a similar example of product inhibition with Pd, see: (b) Phua, P. H.; Mathew, S. P.; White, A. J. P.; de Vries, J. G.; Blackmond, D. G.; Hii, K. K. Elucidating the Mechanism of the Asymmetric Aza-Michael Reaction. *Chem. - Eur. J.* **2007**, *13*, 4602−4613.
(25) 2 equiv of *n*-BuZnBr were used instead of 3 equiv in order to slow down the high catalyst loading reactions.
(26) The addition of 40 equiv of Hg to the reaction relative to Ni resulted in no change on the rate of formation of **2**, suggestive of homogeneous catalysis. For a reference on Mercury Test, see: Chernyshev, V.; Astakhov, A.; Chikunov, I.; Tyurin, R.; Eremin, D.; Ranny, G.; Khrustalev, V.; Ananikov, V. Pd and Pt Catalyst Poisoning in the Study of Reaction Mechanisms: What Does the Mercury Test Mean for Catalysis? *ACS Catal.* **2019**, *9*, 2984−2995.

https://dx.doi.org/10.1021/jacs.0c02237
J. Am. Chem. Soc. 2020, 142, 8928−8937

(27) A first-order dependence on [Fro-DO] was observed between 3 and 12 mM using the Burés method of kinetic analysis (see Section IV-B of the Supporting Information).
(28) (a) MacDonald, D. J. Absorption Spectra of Square-Planar Complexes of Ethylenebisbiguanide with Nickel(II) and Palladium-(II). *Inorg. Chem.* **1967**, *6*, 2269−2270. (b) Hipler, B.; Uhlig, E.; Vogel, J. Binukleare Organonickel(II)-Verbindugen. *J. Organomet. Chem.* **1981**, *218*, C1−C4.
(29) Lin, B.; Clough, C.; Hillhouse, G. Interactions of Aziridines with Nickel Complexes: Oxidative-Addition and Reductive-Elimination Reactions That Break and Make C−N Bonds. *J. Am. Chem. Soc.* **2002**, *124*, 2890−2891.
(30) Oxidative addition can be achieved in an olefin-free system. Treating $Ni(acac)_2$ with *n*-BuZnBr (2 equiv) and aziridine **1** (1 equiv) gives intermediates **A** and **B**, as observed by ^{19}F NMR (Figure S24).
(31) Based on M06 calculated free energies, association of Fro-DO to Ni intermediate **A** is favorable (G = −2.1 kcal/mol). See Section VII-B of the Supporting Information.
(32) (a) PhZnBr was generated *in situ* from equimolar amounts of $ZnPh_2$ and $ZnBr_2$ and stirred for 15 min prior to addition to the catalytic reaction. (b) Addition of up to 3 equiv of $ZnBr_2$ resulted in no ring opening of an *in situ* generated **A** ruling out a peak shift in the catalytic reaction resulting from $ZnBr_2$.
(33) Oxidative addition of aziridine **1** with Ni^0 likely proceeds *via* an irreversible SET. See ref 10. We note that there is some ambiguity regarding whether Fro-DO is bound during the oxidative addition. Ni(0) would be expected to sit as the Fro-DO bound species due to effective π-backbonding. However, this bound species would be significantly deactivated towards oxidative addition. It is thus unclear whether oxidative addition occurs through Fro-DO bound Ni(0) or through a minor equilibrium with Fro-DO-free Ni(0).
(34) For experiments establishing equilibrium between Ni intermediates **A** and **B**, see Section VI of the Supporting Information.
(35) For a treatment of the sulfonamide as anionic, see Section VII-J of the Supporting Information.
(36) Espinet and co-workers evaluated the effect of various EDOs on C−C reductive eliminations from Pd by DFT. See: Pérez-Rodríguez, M.; Braga, A.; Garcia-Melchor, M.; Pérez-Temprano, M. H.; Casares, J. A.; Ujaque, G.; de Lera, A. R.; Alvarez, R.; Espinet, P. C-C Reductive Elimination in Palladium Complexes, and the Role of Coupling Additives. A DFT Study Supported by Experiment. *J. Am. Chem. Soc.* **2009**, *131*, 3650−3657.
(37) Tolman, C. A. Olefin Complexes of Nickel(0). III. Formation Constants of (Olefin)bis(tri-*o*-tolyl phosphite)nickel Complexes. *J. Am. Chem. Soc.* **1974**, *96*, 2780−2789.
(38) This observation agrees with the zeroth-order kinetic dependence on [Fro-DO].
(39) Increasing dimethyl fumarate ligand loading negatively impacts the rate of aziridine **1** consumption. This is likely a result of an off-cycle NiL_2 species which does not undergo oxidative addition to aziridine **1**.
(40) (a) Chatt, J.; Duncanson, L. A. Olefin Co-Ordination Compounds. Part III. Infra-Red Spectra and Structure: Attempted Preparation of Acetylene Complexes. *J. Chem. Soc.* **1953**, 2939. (b) Dewar, M. J. S. A Review of π-Complex Theory. *Bull. Soc. Chem. Fr.* **1951**, *18*, C79.
(41) For an example of second-order perturbation theory analysis, see: Singh, S. K.; Das, A.; Breton, G. W. An Ab Initio Study of the Effect of Substituents on the n→π^* Interactions between 7-Azaindole and 2,6-Difluorosubstiuted Pyridines. *J. Phys. Chem. A* **2016**, *120*, 6258−6269.
(42) (a) In our original report we provided evidence against sulfonyl coordination after observing that the sulfonyl groups of Fro-DO were more than 4 Å from the Ni^0 center in an X-ray crystal structure of Ni(cod)(Fro-DO). However, sulfonyl coordination should be more favorable for a Ni^{II} species than a Ni^0. (b) DFT predicts that the sulfonyl−Ni interaction strengthens in the C−C reductive elimination transition state where the Ni−O distance is shortened to 2.06 Å.

https://dx.doi.org/10.1021/jacs.0c02237
J. Am. Chem. Soc. 2020, 142, 8928−8937